Supplemental Materials

Lead-free Germanium Iodide Perovskite Materials for Photovoltaic Application

Thirumal Krishnamoorthy, Hong Ding, Chen Yan, Wei Lin Leong, Tom Baikie, Ziyi Zhang, Matthew Sherburne, Shuzhou Li, Mark Asta, Nripan Mathews, Subodh G. Mhaisalkar

Experimental Section

1. Chemical

HI (puriss. p.a. >=67%), H_3PO_2 (50% wt. % in H_2O), GeO_2 (>=99.99%) and CsI (99.999%) were purchased from Sigma Aldrich and used as received. CH_3NH_3I was purchased by Dyesol and $HC(NH_2)_2I$ was prepared in our lab as reported in our previous work.

2. Synthesis

Close to 1g of each perovskite salt was synthesized per batch. Aqueous HI (1.5 ml) was mixed with deionized water (1 ml) and aqueous H_3PO_2 (1 ml), forming a colorless solution. GeO_2 (104 mg, 1 mmol) was mixed in the solvent mixture and dissolved by heated up to 90 ^oC using an oil bath. After about 10 min, the solutions turned lemon-like yellow. Three different iodide salts were added in different batch. Upon the addition of solid CsI (260 mg, 1 mmol), a black solid precipitated immediately. Upon the addition of solid CH_3NH_3I (159 mg, 1 mmol), a dark red solid precipitated immediately. Upon the addition of solid $HC(NH_2)_2I$ (172 mg, 1 mmol), an orange solid precipitated immediately. The solutions were cooled down to room temperature without stirring. During cooling, more dark red precipitate and orange precipitate formed while black precipitate remained the same. The solutions went through centrifuge, and the top supernatant solvent was removed. The left crystals were washed with a minimum quantity of dried ethanol. Synthesis was done under inert atmosphere. The final products were dried in vacuum at room temperature for 24 hours.

$CsGeI_3$: Yield 85-95%. FTIR, KBr, cm^{-1}: 744m, 871s, 960w, 1522m, 1623m, 2350w, 3394br, 3736m EDS (Atomic%): Cs: 16.54% (20%); Ge: 20.24% (20%); I: 63.22% (60%).

$MAGeI_3$: Yield 85-95%. FTIR, KBr, cm^{-1}: 906s, 962w, 992w, 1247m, 1458s, 1490m, 2350w, 2706w, 2963w, 3108br, 3751m EDS (Atomic%): Ge: 25.47% (25%); I: 74.53% (75%)

$FAGeI_3$: Yield 85-95%. FTIR, KBr, cm^{-1}: 812w, 1048br, 1351m, 1398m, 1616br, 1712s, 2350w, 3267m, 3394w EDS (Atomic%): Ge: 25.31% (25%); I: 74.69% (75%)

3. Characterization

Powder X-ray diffraction: Phase purity was confirmed by powder X-ray diffraction (PXRD) patterns collected with a Bruker D8 Advance diffractometer (Bragg-Brentano geometry) equipped with a Cu *Kα* X-ray tube operated at 40 kV and 40 mA using a step size of 0.02° and a time per step of 1 s. The powder samples were mounted in a Bruker air-sensitive sample holder and under these conditions; the intensity of the strongest reflection was approximately 2000 counts. Variable temperature powder X-ray diffraction patterns were collected on a # diffractometer (Cu *Kα*, 40 kV and 40 mA; step size of 0.02° time per step of 0.5s) from room temperature 25 °C to 150 °C. Experimental fitting of the data was carried out from 10-60° 2θ using *TOPAS V4.1*.[1] The lattice parameters of the $AGeI_3$ (A = Cs, MA and FA) perovskite were extracted via a Pawley fit and compared with the literature reported values.

Energy-dispersive X-ray (EDX) spectroscopy was conducted to analyze the chemical composition of the powder samples under an accelerating voltage of 20 kV. UV-VIS-NIR spectrophotometer (Shimadzu UV-3600) was used to measure the transmission

and reflectance spectra of thin film samples in the wavelength range of 300 nm to 800 nm at room temperature with an integrating sphere attachment (ISR-3100). The reflectance standard was a highly refined barium sulfate powder (Wako, pure).

Thermogravimetric analysis was performed on a TGA Q500 V6.7 (TA Instruments) over a temperature range from 27 ^{o}C to 800 ^{o}C at a ramp of 10 ^{o}C/min under nitrogen atmosphere. Differential scanning calorimetry was conducted on a Q10 V9.9 Build 303 calorimeter (TA Instruments) at a rate of 10 ^{o}C/min under nitrogen, where the minimum temperature was -50 ^{o}C and the maximum temperature was the decomposition temperature of the corresponding perovskite.

Fourier Transform Infrared spectra of powder samples were collected using Frontier FT-NIR/MIR Spectrometers (Perkin Elmer) across a wavelength range of 600 to 4000 nm with the Universal ATR attachment.

Photo Electron Spectroscopy in Air (PESA) measurements was recorded with a Riken Keiki AC-2 PESA spectrometer with a power setting of 800 nW and a power number of 0.5. Samples for PESA were prepared by filling the metal sample holder with powder samples of perovskites.

The solar cells were characterized by both current-voltage curves and incident photon-to-current efficiency (IPCE) spectra. An Agilent 4155C analyzer was used to measure the current-voltage curves under AM 1.5G simulated illumination from a solar simulator (San-EI Electric, XEC-301S). A lock-in amplifier (Stanford Research Systems, SRS 810) was used to measure the IPCE spectra with a white light channeled from a Newport 300 W Xenon lamp and through a 17 Hz mechanical chopper wheel and a monochromator (Oriel Cornerstone 130). No bias light was applied.

4. Device fabrication

Fluorine-doped tin oxide-coated glass substrates were etched with zinc powder and HCl (2M), resulted in the formation of the desired electrode pattern. These substrates were then cleaned by diluted detergent, deionized water and ethanol under ultrasonication. After blew by nitrogen gas, the dried substrates were treated by ozone plasma for 15 min. Titanium diisopropoxide bis(acetylacetonate) solution (75% in 2-propanol) diluted in ethanol (1:9 v/v) was sprayed on the substrates and sintered for 30 min at 500 ^{o}C, forming a blocking layer of TiO_2 (60-70 nm). After cooling to room temperature, the substrates were treated in 40mM $TiCl_4$ solution for 30 min at 70 ^{o}C, followed by the annealing at 500 ^{o}C for 30 min. TiO_2 paste (DYESOL-30NRD) diluted in ethanol (2:7 w/w) was spin-coated onto the blocking layer to form a mesoporous TiO_2 layer. The substrates were treated in 20 mM $TiCl_4$ solution at 70 °C for 30 min and annealed at 500 °C for 30 min before the deposition of the germanium based perovskite.

Solution was prepared by dissolving solid perovskite (1M) in DMF and filtered using 0.2 um filter. The filtered solution was deposited on the TiO_2 substrates by spin coating at 4000 rpm for 30 sec, followed by annealing the samples at 70 ^{o}C for 10 min. Spiro-OMeTAD was dissolved in chlorobenzene (70 mg/ml) and spin-coated on the substrates, forming a hole transporting layer. Au electrodes were deposited on these substrates by thermal evaporation.

Computational Session

First-principles Calculations

Cubic AMX_3-type halide perovskite structures were first relaxed to the equilibrium lattice constants with density-functional-theory calculations. These calculations were performed with the Perdew-Burke-Ernzerhof (PBE) generalized gradient approximation [4] and projector augmented wave potentials [5-6], as implemented in the Vienna ab initio simulation package [7]. The calculations made use of a plane-wave cutoff energy of 520 eV and a 12×12×12 Monkhorst-Pack k-point sampling mesh[2]. All structures were relaxed with conjugate-gradient algorithm until the total energy of unit cell converged within 10^{-4} eV. Several numerical tests were performed to estimate the convergence of calculated bandgap values with respect to the plane-wave cutoff and k-point density. On the basis of these tests, the calculated bandgap values are estimated to be converged numerically to within a precision of approximately 0.01 eV.

As described in the main text, to provide an additional set of results for the computational screening efforts, we also employed the Δ-sol method [8] as a framework for high-throughput calculations of bandgap values for candidate compounds. The Δ-sol method has been developed to predict bandgap values based on the energy changes resulting from addition or subtraction of

electrons in a DFT-based calculation. The method thus features computational costs comparable to standard PBE calculations, but with an accuracy that has been demonstrated to be highly improved [8]. In the current implementation of the Δ-sol method, we chose N^*= 68 and 72 for *sp* and *spd* bonded systems with PBE functionals, respectively. We fixed cell volume and shape, as well as internal atomic positions, for the total energy computations of systems with additional or removed electrons.

Computational Screening

As we are interested in identifying compounds for solar absorber applications, the computational screening began with a survey of calculated bandgap values. Specifically, the exercise aimed to identify compositions having appropriate band gaps for photon absorption in the solar spectrum, i.e., in the range of 1.1-1.5 eV. In the present work, calculated bandgap values from PBE calculations (E_g^{PBE}) were first used to assess bandgap trends across 360 AMX_3 compositions, with the results shown in Figure 1. Some general trends in the computed E_g^{PBE} values with varying A and X site compositions are found: the computed values of E_g^{PBE} increase as the A site element changes from K to Cs, while it decreases as the X site element changes from Cl to I. This relationship is in general correlated with atomic size effects on lattice parameters of the crystal structure, as well as the corresponding electronegativity change in a given column of the periodic table.

For screening purposes we searched for the AMX_3 compositions with PBE-calculated bandgap values in the range of 0.2-0.7 eV. As explained in the main text, this range of PBE bandgap values was identified to be within approximately 60 % of the values calculated for $CsSnI_3$, where previous experimental measurements reported bandgap values appropriate for solar light absorption applications. Computed lattice constants (*a*) and PBE bandgaps (E_g^{PBE}) of the nine new AMX_3 compositions identified through this procedure, along with the corresponding results for $CsSnI_3$, are listed in Table S1. We found that the M-site element of these 9 compounds is either Sn or Ge.

As found for $CsSnI_3$, the calculated values of E_g^{PBE} are expected to underestimate significantly the true bandgaps of the compounds considered in this work. Therefore, another computational approach, i.e. the Δ-sol method [4], was employed as an independent method for exploring the trends of bandgap values across different candidate compounds. The Δ-sol method is a semi-empirical computational approach that has been shown to yield improved predictions of bandgap values ($E_g^{\Delta-sol}$) with a computational cost that is comparable to PBE and thus appropriate for high-throughput screening [4]. We performed Δ-sol calculations for all of the candidates AMX_3 compounds for which $E_g^{PBE} > 0.1$ eV. In Table S1 we list calculated $E_g^{\Delta-sol}$ values for the subset of 10 compounds listed in the previous paragraph. The Δ-sol calculated bandgaps were found to be uniformly larger than those derived from PBE, and for $CsSnI_3$ the method overestimates the measured bandgap by 0.6 eV. Although the Δ-sol bandgap values are larger than those derived from PBE, the trends across the different compound chemistries predicted by these two computational methods were found to be similar. Specifically, we computed the Spearman rank correlation coefficient between the computed values of E_g^{PBE} and $E_g^{\Delta-sol}$, and found that the relationship between these two sets of calculations can be well described using a monotonic function, i.e. the rankings of predicted bandgap values using these two different methods are highly correlated with a Spearman coefficient of 0.95.

To further down-select the compounds identified through the computational screening of bandgaps, we next focused on predictions of thermodynamic stability, based on calculated values of the "energy above the hull" (ΔE_H). This quantity is defined to be the difference in energy between a candidate compound, and the compound or phase-separated set of compounds that give the lowest energy for the same overall composition. Thus defined, non-zero (positive) values of ΔE_H indicate that the compound is energetically unstable with respect to formation of another compound with the same composition, or with respect to phase decomposition to a set of compounds with different individual compositions. In the present work we made use of the Materials Project database[3] to determine whether each of the 10 AMX_3 compounds in Table S1 are thermodynamically stable based on the calculated value of ΔE_H. It is worth noting that in this exercise the energies of the candidate AMX_3 compounds were all considered with the cubic perovskite phase. The resulting computed values of ΔE_H are shown in Table S1 and they indicate that among these 9 compositions identified (i.e., other than $CsSnI_3$), only three of them, namely $RbSnBr_3$, $CsGeI_3$ and

$CsSnBr_3$, have calculated values of ΔE_H=0, indicating that these are the only three that have energies consistent with low-temperature phase stability.

In summary, the computational screening based on PBE-calculated bandgaps and calculated energetic stability yielded the identification of three candidate perovskite compounds as being of interest for potential solar-cell applications: $RbSnBr_3$, $CsGeI_3$ and $CsSnBr_3$. It is important to note that the same three compounds were found when the bandgap screening was based on the identification of Δ-sol values that were within 20 % of that calculated for $CsSnI_3$, rather than the use of PBE values. Thus, although neither the PBE nor Δ-sol methods yield bandgap values in quantitative agreement with experimental measurements, they lead to similar predictions when exploring trends in bandgap values across the range of compound chemistries considered in the computational screening exercise.

Table S1: Calculated lattice constants (a), bandgap values based on the PBE (E_g^{PBE}) and Δ-sol ($E_g^{\Delta-sol}$) methods, and thermodynamic quantity "energy above hull" ΔE_H) of nine selected ABX_3 compositions.

A	M	X	a (Å)	E_g^{PBE} (eV)	$E_g^{\Delta-sol}$ (eV)	ΔE_H(meV/atom)
Cs	Sn	I	6.28	0.44	1.91	0
Rb	Sn	I	6.25	0.38	1.89	8.8
Rb	Sn	Br	5.87	0.57	2.26	0
Rb	Ge	I	5.96	0.55	1.91	28.4
K	Sn	I	6.23	0.35	1.88	48.7
K	Sn	Br	5.85	0.53	2.25	42.1
K	Ge	I	5.92	0.49	1.90	61.7
K	Ge	Br	5.53	0.57	2.32	10.8
Cs	Ge	I	5.99	0.62	1.93	0
Cs	Sn	Br	5.89	0.65	2.27	0

Band Structure Calculation of $MAGeI_3$

We also explored the band structure and electronic properties of $MAGeI_3$. In the present work, the structure of $MAGeI_3$ was modeled in a cubic cell with lattice constant of a = 6.12 Å, in correspondence with the experimentally measured lattice parameters of the rhombohedral cell at room temperature, as shown in Fig. 2(b) and Fig. 3(a). The MA molecule was initially placed in the center of the cell, and oriented along the (100) direction, and the atomic coordinates were fully relaxed. Computed band structures along the high-symmetry directions in the cubic structure and the projected density of state of $MAGeI_3$ are plotted in Fig. S2. Similar to the band structure of $CsGeI_3$ shown in Fig. 3(b), the direct bandgap (E_g^{PBE} =1.01 eV) is also located at the R point of Brillouin zone and the bandgap is mainly attributed to the Ge "intra-atomic" bonding-antibonding splitting. The calculated bandgap difference between $MAGeI_3$ and $CsGeI_3$ is 0.39 eV, which agrees well with the experimental measurement of 0.37 eV shown in Fig. 3 (a).

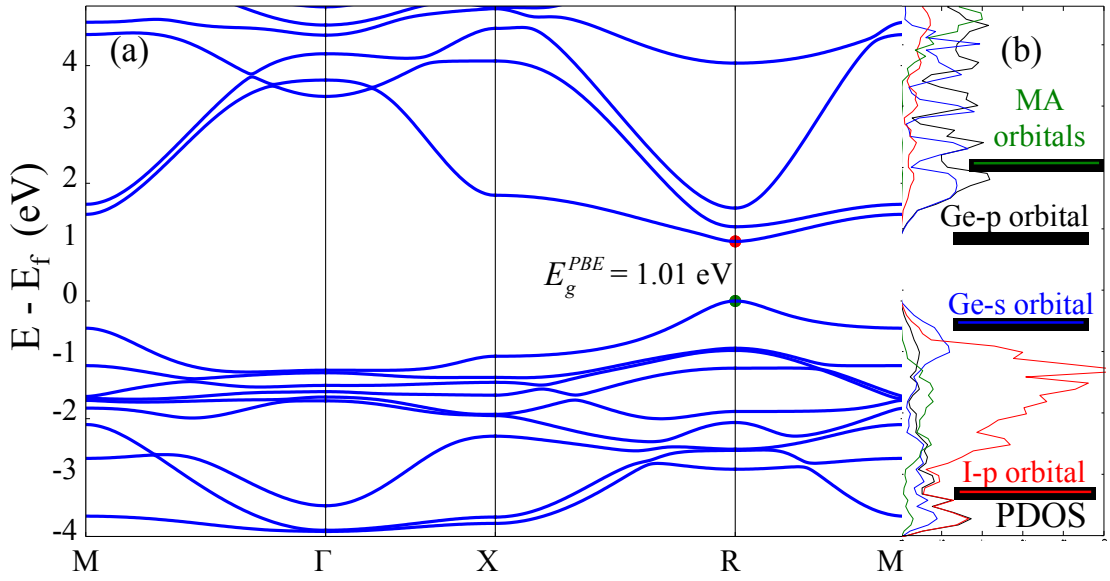

Figure S2 : (a) The band structure of cubic $MAGeI_3$ calculated with PBE functional. (b) Atom projected density of states. The energy of the highest occupied state is set to 0 eV.

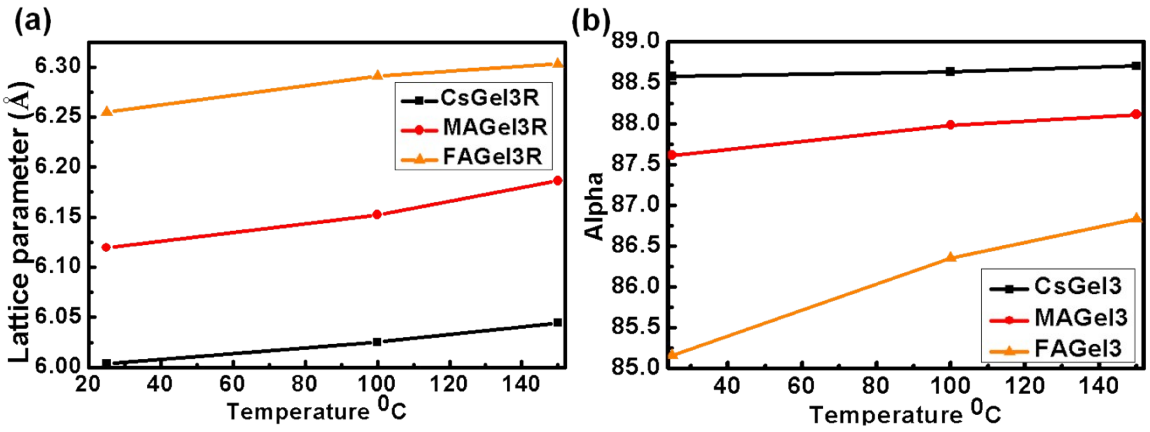

Figure S3. (a)Lattice parameter of rhombhohedral crystal structure. (b) Lattice angle of rhombhohedral crystal structure

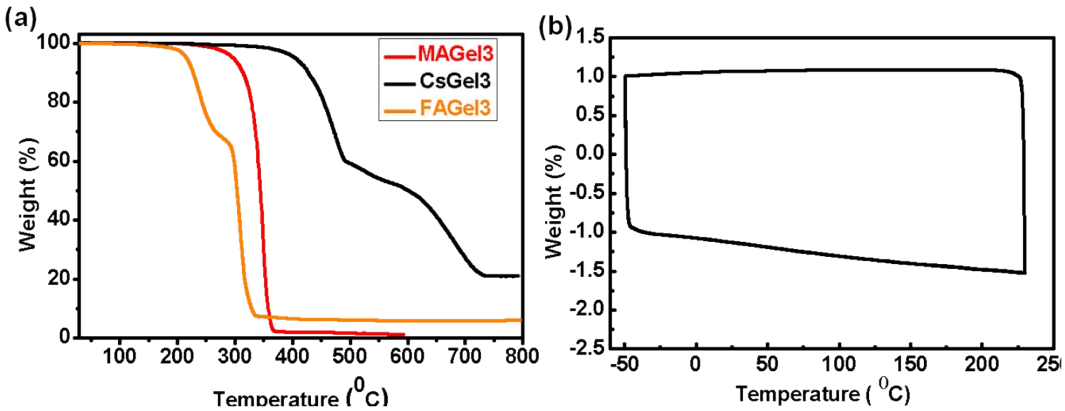

Figure S4. (a) Thermogravimetric analysis (TGA) thermogram of Germanium perovskites. (b) Differential scanning calorimetry of representative CsGeI3

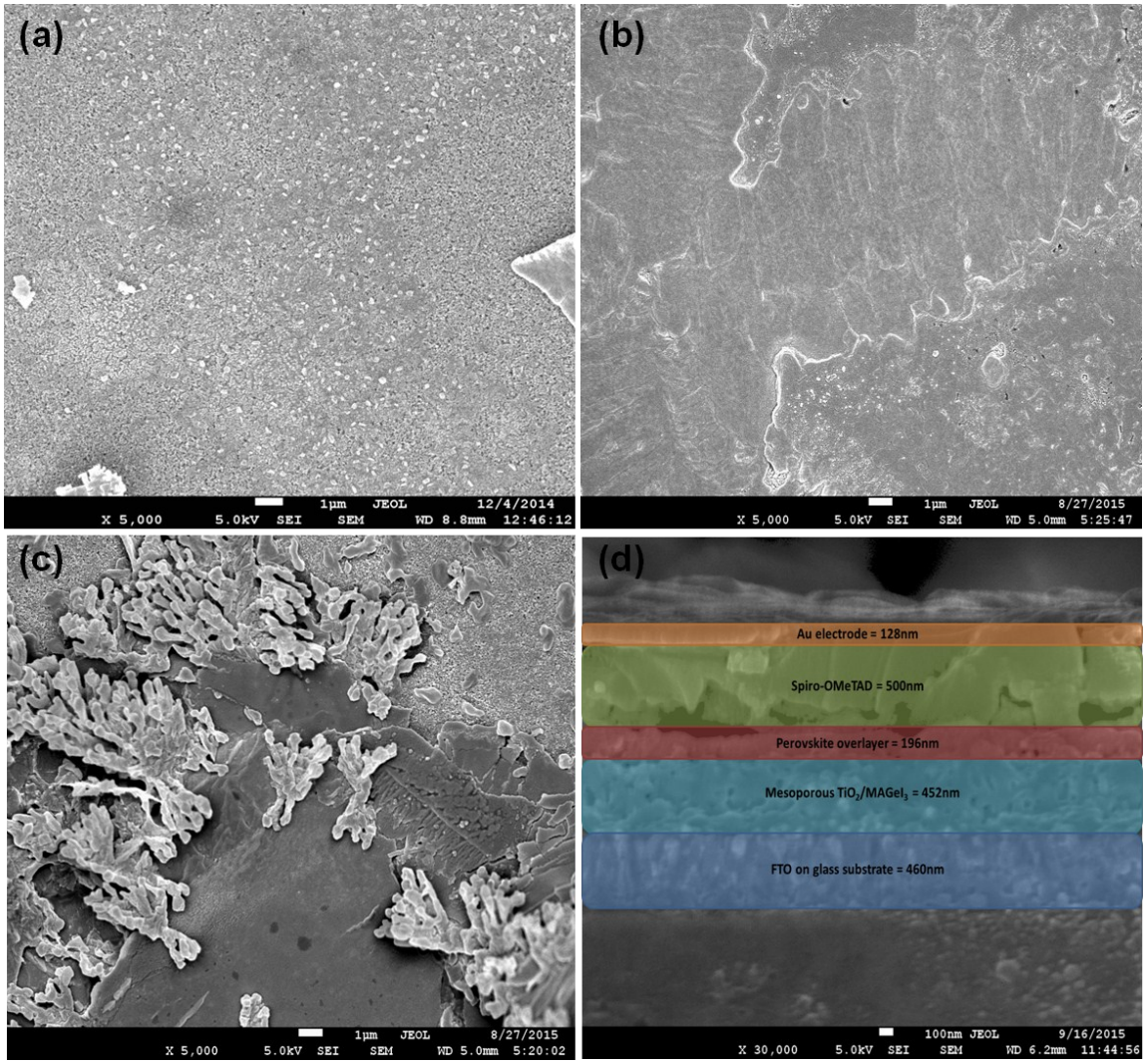

Figure S5. SEM images showing top view of thin film of (a) $CsGeI_3$, (b) $MAGeI_3$, and (c) $FAGeI_3$. (d) Show the cross-section view of device.

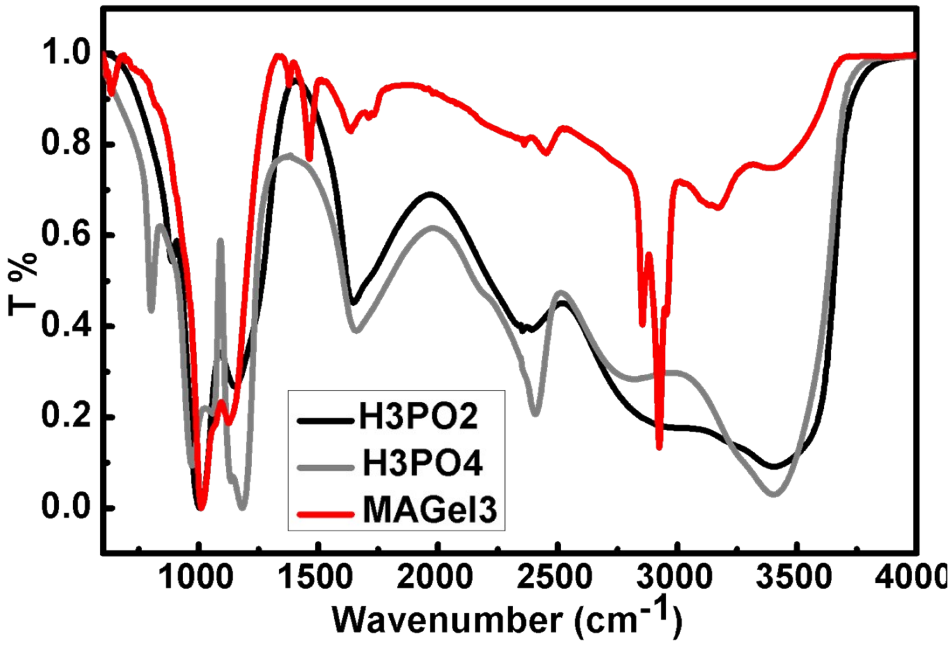

Figure S6. Fourier transform infrared spectroscopy (FTIR) spectra of $MAGeI_3$ and phosphorous oxoacids.

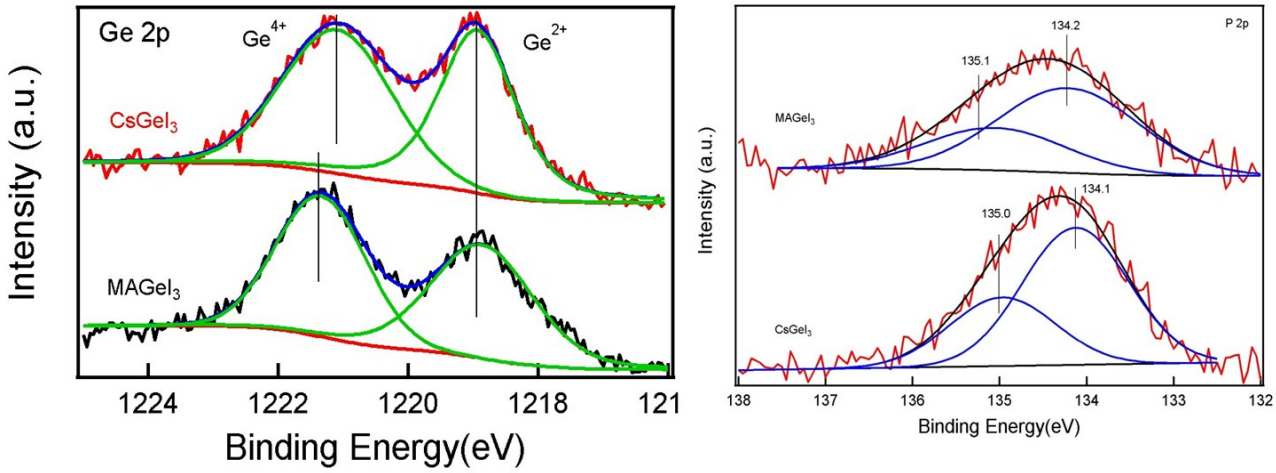

Figure S7. XPS narrow scans of $CsGeI_3$ and $MAGeI_3$ for Ge 2P and P 2p.

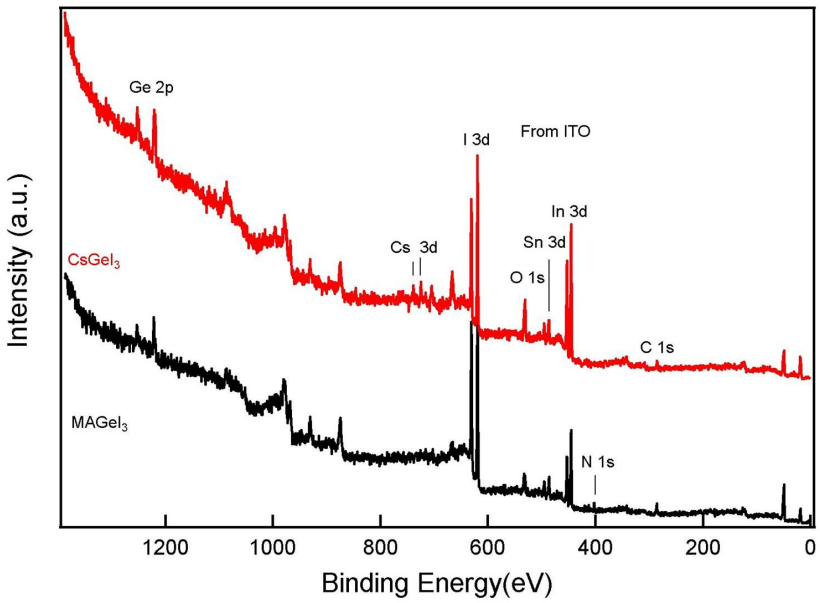

Figure S8. Widescan of CsGeI3 and MAGeI3 samples

(1) Bruker; Bruker AXS Inc.: Madison, Wisconsin, USA, 2008.

(2) Monkhorst, H. J.; Pack, J. D. *Phys Rev B* **1976**, *13*, 5188.

(3) Jain, A.; Ong, S. P.; Hautier, G.; Chen, W.; Richards, W. D.; Dacek, S.; Cholia, S.; Gunter, D.; Skinner, D.; Ceder, G.; Persson, K. A. *Apl Mater* **2013**, *1*.

(4) Perdew, J. P.; Burke, K.; Ernzerhof, M. *Phys Rev Lett* **1996**, *77*, 3865.

(5) Blöchl, P. E. *Physical Review B* **1994**, *50*, 17953.

(6) Kresse, G.; Joubert, D. *Physical Review B* **1999**, *59*, 1758.

(7) Kresse, G. *J Non-Cryst Solids* **1995**, *193*, 222.

(8) Chan, M. K. Y.; Ceder G. Phy. Rev. Lett. 2010, 105, 196403